# High precision and continuous field measurements of δ 13C and δ 18O in carbon dioxide with a cryogen-free QCLAS

**Journal Article**

**Author(s):**
Tuzson, Béla; Mohn, Joachim; Zeeman, Matthias J.; Werner, Roland A.; Eugster, Werner (iD); Zahniser, Mark S.; Nelson, David D.; McManus, John B.; Emmenegger, Lukas

**Applied Physics B**
Lasers and Optics

B. TUZSON[1]✉
J. MOHN[1]
M.J. ZEEMAN[2]
R.A. WERNER[2]
W. EUGSTER[2]
M.S. ZAHNISER[3]
D.D. NELSON[3]
J.B. MCMANUS[3]
L. EMMENEGGER[1]

# High precision and continuous field measurements of $\delta^{13}$C and $\delta^{18}$O in carbon dioxide with a cryogen-free QCLAS

[1] Empa, Swiss Federal Laboratories for Materials Testing and Research, Laboratory for Air Pollution and Environmental Technology, Überlandstr. 129, 8600 Dübendorf, Switzerland
[2] ETH Zurich, Institute of Plant Sciences, Grassland Science Group, Universitätsstr. 2, 8092 Zürich, Switzerland
[3] Aerodyne Research Inc., 45 Manning Road, Billerica, MA 01821, USA

**ABSTRACT** The present paper describes a compact and cryogen-free, quantum cascade laser based absorption spectrometer (QCLAS) designed for in situ, continuous and high precision isotope ratio measurements of atmospheric $CO_2$. The mobile instrument incorporates several new features including a novel astigmatic multi-pass cell assembly, a quasi-room temperature quantum cascade laser, thermoelectrically cooled detectors as well as a new retrieval approach. The combination of these features now makes it possible to measure isotope ratios of ambient $CO_2$ with a precision of 0.03 and 0.05‰ for $\delta^{13}$C and $\delta^{18}$O, respectively, using a 100 s integration time. A robust and optimized calibration procedure was developed to bring the retrieved isotope ratios on an absolute scale. This assures an accuracy better than 0.1‰ under laboratory conditions. The instrument performance was also assessed in a field campaign in which the spectrometer operated autonomously and provided mixing ratio values for the main three $CO_2$ isotopologues at one second time resolution. An accuracy of 0.2‰ was routinely obtained for both isotope ratios during the entire period. The results were in excellent agreement with the standard laboratory-based isotope ratio mass spectrometer measurements made on field-collected flask samples. A few illustrative examples are used to depict the potential of this optical method in atmosphere–biosphere research.

## 1 Introduction

The accentuated concentration increase of carbon dioxide and other trace gases in the Earth's atmosphere has led to concern about the potentially profound consequences of amplified greenhouse warming. While the majority of the existing measurements clearly indicate that the current increase in atmospheric $CO_2$ concentration is mainly driven by the combustion of fossil fuel, it is still difficult to account for the fate of anthropogenic $CO_2$ in every detail. The key question of "How is this additional $CO_2$ distributed amongst the atmosphere, oceans and terrestrial biosphere?" needs to be answered [1]. Thus, a detailed understanding of the inter-

actions among the atmosphere and biosphere is essential for interpreting the role of terrestrial ecosystems on global carbon dynamics [2–5]. The analysis of both the concentrations and stable isotope ratios of atmospheric $CO_2$ provides important information for quantifying ecosystem–atmosphere interactions [6–8]. However, this generally requires extensive and long term $CO_2$ sampling under field conditions. Yet acquiring large numbers of samples to analyze has been a challenge, mostly because of the employed measurement technique. The standard analytical tool for the determination of stable isotope ratios in trace gases is the isotope-ratio mass spectrometer (IRMS), which, despite its very high precision, is not well suited for field deployment. Therefore, there is a need to further refine current and/or develop new measurement techniques and calibration approaches which allow for continuous, high-precision isotope ratio measurements at high repetition rates. As an alternative analytical method to conventional IRMS, laser absorption spectroscopy has been several times applied to retrieve isotope ratios in atmospheric measurements [10–14]. Being an optical method employed in the mid-IR spectral region, where the majority of trace gas molecules have their characteristic fingerprint structure, it inherently allows to distinguish between molecules having identical mass or being structural isomers. Because it does not require special sample preparation, non-destructive in situ measurements on a timescale of seconds can be achieved. This makes the technique well suited for trace gas flux measurements and airborne applications.

Depending on the spectral region of interest, several laser based light sources are available in the mid-IR, which have successfully been employed for isotopologue selective absorption spectroscopy: difference frequency generation [15, 16], lead-salt diodes [17–20], color-center lasers [21], gas lasers [22] and quantum cascade lasers [23–25]. The latter are particularly attractive because of their stable single mode spectral output, high power and near room temperature operating conditions.

This paper describes a new approach using direct absorption laser spectroscopy employing a pulsed quantum cascade laser (QCL) which operates near 4.3 μm at quasi-room temperature. The instrument was designed and developed in a common effort with Aerodyne Research Inc. A detailed description of the instrument design and signal processing has already been discussed in a previous paper [9]. Here, we focus

✉ Fax: +41-44-8216244, E-mail: bela.tuzson@empa.ch

on recent advances and improvements that make the instrument completely cryogen-free while maintaining the same level of performance. This implicitly involves an enhancement in the instrument performance of a factor of three at least. Furthermore, a calibration procedure will be presented which allows bringing the retrieved isotope ratios on an absolute, internationally accepted scale even for long-term field measurements. Finally, the laser spectrometer is validated in a field campaign by comparing its output with IRMS measurement values. Details about laboratory investigations, measurement strategy and field application will be presented in the following sections.

## 2 Experimental

### 2.1 *Spectrometer setup*

The optical module (Fig. 1) of the instrument was designed to be compact and minimize the negative aspects of pulsed laser operation. Driving the laser with short (typically 10 ns) pulses has the advantage of significant suppression of optical interference fringes compared to continuous wave lasers [26]. On the other hand, additional noises like pulse-to-pulse output energy fluctuation and broad laser line width, are limiting factors in performing high precision measurements with such laser sources [27]. This limitation was significantly reduced by combining the dual, reference and sample absorption cell approach with a new spectral analysis method. Briefly, the laser beam emitted by the QCL (Alpes Lasers) is first collimated by a reflecting objective and then split in two parts of equal intensities by a wedged ZnSe beamsplitter. Each beam is coupled in one of the multi-pass cells and finally focused onto the detector. The dual-cell arrangement allows for simultaneous sample/reference gas measurements and, hence, improves the accuracy of the isotope ratio measurement since the sample mixing ratios are continually referenced to the stable isotope ratios in the reference gas. Uncertainties in the spectral fitting procedure are considerably reduced by applying the spectral analysis to the ratio of the sample and reference spectra.

In a previous feasibility study on isotope ratio measurements we showed that it is possible to select a spectral range near $2310\,\mathrm{cm}^{-1}$ that allows, despite the limited tuning rate of QC lasers, the simultaneous quantification of the three main $CO_2$ isotopologues: $^{12}C^{16}O_2$, $^{13}C^{16}O_2$ and $^{12}C^{16}O^{18}O$ [28]. It was also recognized that the best performance is obtained with a relatively short path length (5 to 10 m) and a gas pressure of about 8 kPa. This is an optimal tradeoff between selectivity and sensitivity when using pulsed QC lasers. At these conditions the molecular absorption line width more closely matches the laser line width ($> 0.01\,\mathrm{cm}^{-1}$), but there is still an adequate separation of the $CO_2$ lines, and the contribution of wing effects from the neighboring absorption features is minimal. Furthermore, the observed optical depth for all three $CO_2$ isotopologues is close to 10%. This has the advantage of substantially reducing the quantification problems due to possible detector non-linearity effects. However, the similar absorbance implies that the line strengths and therefore the ground state energies for the main and minor isotopic species, are different. Thus, the instrumental precision tends to suffer from a larger temperature sensitivity. An uncompensated thermal drift of one degree in the instrument will influence the measured isotope ratio value by 12 and 18‰ for $\delta^{13}C$ and $\delta^{18}O$, respectively [28]. This sensitivity is diminished by using the spectral ratio method, because the line strength temperature dependence enters as a ratio, and hence the derived isotope ratio is sensitive to the temperature difference between the two cells rather than their absolute temperatures. This also minimizes second order effects such as changes in absorption line shape with pressure and temperature [9].

The above mentioned issues are addressed in various ways. First, two small (300 ml) volume astigmatic multi-pass absorption cells (AMAC-36, Aerodyne Research Inc.) are modified to provide the optimal path length of 7.3 m. This was easily achieved by rotating the back mirror until the astigmatism is minimal and then slightly tilting the mirror so that an elliptical spot pattern appears. Secondly, the original glass tube of the cell was replaced by a custom-made aluminum tube with a profile as depicted in Fig. 2. The inner, cylindrical side is Teflon coated to assure a chemically inert surface and to avoid potential memory effects due to surface irregularities. As a secondary effect, the 25 µm thick coating helps to prevent unwanted back-reflections (fringing effect) within the cell from the otherwise strongly reflective metallic surface. These modified cells are then positioned adjacent to each other and a thin layer of heat sink compound is applied between the contact surfaces to assure an effective thermal coupling of the cells. Moreover, the aluminum profiles have a coupling hole at their middle position which allows to insert a temperature sensor directly into the optically active volume. Therefore, we measure the temperature of the gas which actually does the absorption of IR radiation, without being biased
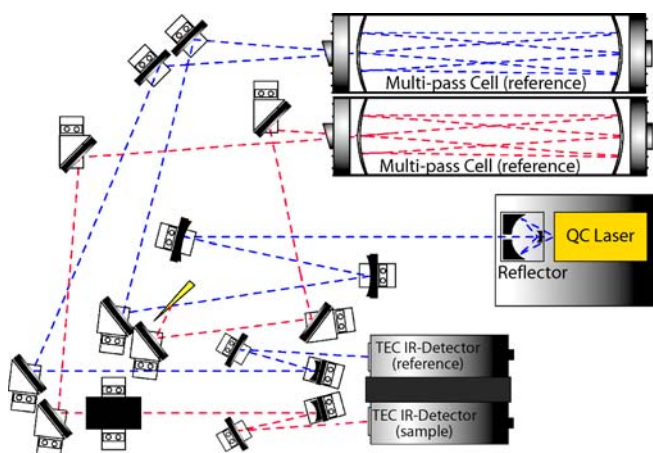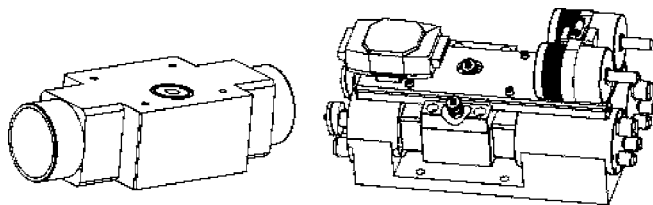


FIGURE 1  Optical setup of the QCLAS



FIGURE 2  The cell-body design and the compact, thermally coupled reference/sample cell assembly with the temperature and pressure sensors mounted at the top

by the cell body or other "inactive" places. A pair of identical, calibrated and high precision 30 kΩ thermistors (Betatherm) are used to monitor any fluctuation in the gas temperature. The sensor signals are immediately digitized by a 16-bit, multi-channel analog-to-digital converter (I-7005, ICP-DAS). The pressure in the cells is measured by two absolute pressure transducers (626A12, MKS Baratron) mounted on the top of the cell assembly. These parameters are then feed into a PC and used by TDLWintel (Aerodyne Research Inc.) for retrieving the concentrations.

## 2.2    *Instrument characterization*

Significant effort was invested to stabilize the instrument against drifts caused by ambient temperature fluctuations and other disturbing influences. The entire optical module was sealed and insulated. The baseplate as well as the cover were maintained at $35 \pm 0.1\,°C$ using thermostatically controlled heaters (CT15122, Minco). Although, the optical path lengths outside the cells are matched to reduce the effects of residual background $CO_2$ absorption, a constant flow of $N_2$ was used to purge the optics and prevent any spurious absorption by ambient $CO_2$. Two fans were added to circulate the air inside the enclosure. The temperature difference between the gases that flow through the sample and reference cells was minimized before entering the optics by using an active temperature controlled "cold plate" (CP15, Lytron) system. The sample and reference gases flowing through these plates, which consist of copper tubes pressed into a channeled aluminum extrusion, are pre-heated so that their temperature closely matches the absorption cell temperature. A constant gas flow through the cells was maintained by mass flow controllers, while the pressure level in the cell was adjusted by high precision flow metering valves. More details are given in the next sections.

Another main issue was to obtain a completely cryogen-free instrument that operates unattended during field measurements. Thus, instead of the standard liquid nitrogen (LN2) cooled detection devices, a new generation of thermoelectrically cooled (TEC) detectors (PVI-3TE-4.4, Vigo System) with miniaturized pre-amplifiers and TEC-controllers (MTCC-01, Vigo System) have been used. These detectors showed good detectivity ($D^* > 5 \times 10^{10}$) and linearity. A pair of matched modules were symmetrically mounted on a common, temperature controlled heat-sink to improve their detection characteristics. It should be, however, recognized that compared to the previous instrument based on LN2 detectors [9], the TEC detectors are more sensitive to changes in the optical alignment for the following reasons: first, they are optically immersed into high refractive index GaAs hyperhemispherical lenses making them sensitive to the aiming angle, and second, the active area is only $0.25\,mm^2$ which makes optical alignment very critical. Changes in the optical system originating from mechanical instabilities (vibrations) or from tiny temperature fluctuations can cause low frequency drifts of the instrument.

The instrument performance in terms of detection limit and long-term stability was characterized by the Allan variance technique [29]. The mixing ratios of the individual $CO_2$ isotopologues were measured with one second
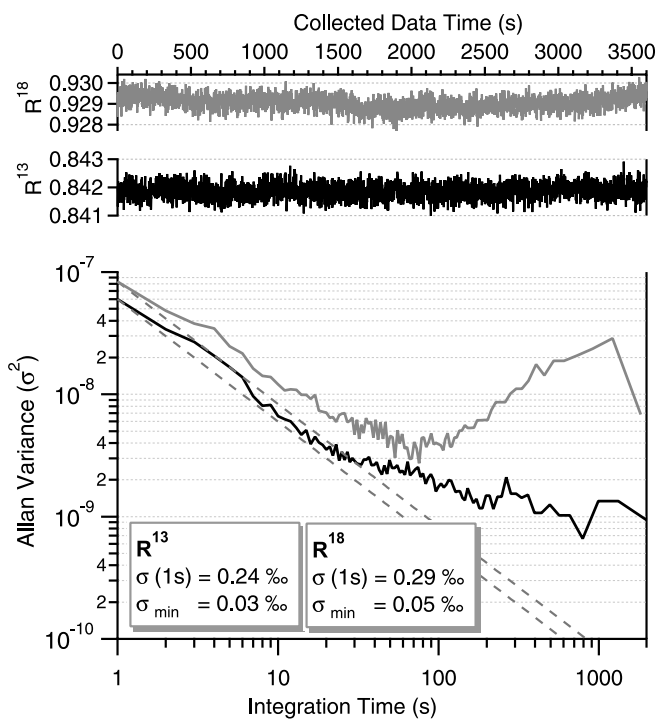


**FIGURE 3**    Time series of isotopic abundance weighted concentration ratios $R^{13}$ and $R^{18}$ as retrieved by the spectrometer and the associated Allan plots

time resolution from a compressed air cylinder over a one hour period. The isotopologue concentrations reported here are weighted by their natural abundances as given in the HITRAN database [30]. Time series of the spectroscopically retrieved concentration ratios $R^{13}$ and $R^{18}$ (where $R^{13} = [^{13}CO_2]/[^{12}CO_2]$ and $R^{18} = [^{12}C^{16}O^{18}O]/[^{12}CO_2]$) are shown in Fig. 3. The precision at one second is about 0.3‰ for each ratio. From the associated Allan variance plots an optimum averaging time of the order of 100 s can be derived. This corresponds to a relative precision of 0.03‰ and 0.05‰ for the $R^{13}$ and $R^{18}$ ratio, respectively. For integration times beyond 120 s, the Allan plot shows a horizontal level or even increasing variance, which indicates the presence of $1/f$-type and "drift" noise. Since we compute mixing ratios based on nearly cancelled spectra, proportional noise in the measurement of the integrated absorbances is less important. This relaxes the requirements on the stability of the laser tuning rate, the laser line width and the spectral fitting routines. Therefore, the drift noise is most probably caused by a drift in the temperature difference between the sample and reference cell. Indeed, the Allan plot of the temperature ratio (not shown) also reaches a minimum after 120 s integration time. Its value ($1 \times 10^{-6}$) corresponds to a precision of 0.3 mK in each cell. This is significantly better than what is needed for the temperature measurements to reach a precision of 0.1‰ in the $\delta$-values.

## 2.3    *Calibration method and material*

The application of direct absorption spectroscopy technique is an absolute method that should allow for a straightforward calculation of the concentration, and hence

the isotope ratios from the measured signals. However, the accuracy of this calculation depends on the knowledge of the instrumental laser line width and shape, and the molecular line parameters including line strength, pressure and temperature dependence listed in the HITRAN database. Additionally, instrumental non-linearity, non-unity gain factors and potential cross-coupling effects could bias the retrieved isotope ratio values. Therefore, the instrument needs to be equipped with a system to calibrate the entire setup and retrieval method. In fact, it was previously found [9] that the retrieved isotope ratios are dependent on the $CO_2$ concentration. Since this behavior is not completely understood yet, one can only speculate about the cause. A subtle effect like asymmetric and changing effective laser line width, which is due to the laser chirp during the scan, may lead to a different response of the isotopologue absorption features to changing concentration, and thus to dependency of the isotope ratio on total $CO_2$. Furthermore, the uncertainty in the spectral baseline may be more relevant at higher $CO_2$ concentrations. The spectral window used in the present experiment is localized between two absorption lines belonging to the main $CO_2$ isotopologue and being ten times stronger than those used for the measurements. Although, at the lower $CO_2$ concentration their interference is small, the tail of the line profile gets more pronounced as the concentration of the absorbing gas increases. If this change in the baseline is not perfectly modeled, it can also lead to non-linearity effects.

In order to investigate the instrument response we used four specially prepared calibration gases with $CO_2$ mixing ratios spanning the range of 1000–1970 ppm and $^{13}C$ of $-37$ to $-4‰$. The preparation procedure of these air tanks has been described in detail by Mohn et al. [31]. The instrumental response to changing $CO_2$ concentration at constant isotopic composition was determined by dynamically diluting the calibration gas with $CO_2$-free air. The retrieved isotope ratio values showed a pronounced linear dependence on the $CO_2$ concentration (Fig. 4a). Follow-up measurements, performed on the other calibration gases with different $^{13}C$-values, revealed a systematic feature of this method. The dilution curve preserved the straight line relationship and beyond that, the slope value remained the same, independent from the isotopic composition of the $CO_2$. The different $CO_2$ isotopic compositions of the various calibration gases were reflected only by the offset between the slopes. Therefore, it is straightforward to "normalize" the spectroscopically measured isotope ratios to an arbitrary selected $CO_2$ concentration (e.g., 400 ppm) and then to determine the calibration function that links their values to the internationally accepted $\delta$-scale. The linearity and potential accuracy of the instrument can be assessed from the residual of the linear fit, which has a $1\sigma$ standard deviation of $0.06‰$ when applied to the above mentioned four reference gases (Fig. 4b).

Based on the results discussed above a slightly modified calibration scheme was designed for field applications. The aim was to speed-up and simplify the calibration while maintaining the required accuracy. Given the linear behavior depicted in Fig. 4, the entire calibration of the spectrometer can in principle be performed by single-point measurements of three adequate reference gases. Two are needed to determine the dependency of isotope ratios on the $CO_2$ concentration
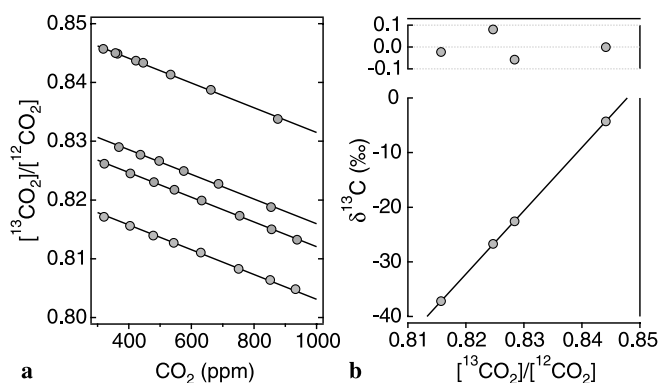


FIGURE 4    (a) Dilution curves of four calibration gases with different $CO_2$ isotopic composition. (b) Comparison of relative isotope ratios determined by QCLAS with the $\delta$-values measured by IRMS

| Tank code | [CO2] (ppm) | $\delta^{13}C$ (‰) | $\delta^{18}O$ (‰) | Remark |
|---|---|---|---|---|
| O1 | $10^6$ | −4.09 | −16.23 | Starting material (Linde) |
| O2 | $10^6$ | −24.86 | −28.24 | Starting material (Messer) |
| A | 400.2 | −9.23 | −7.30 | Calibration $\delta$-scale |
| B1 | 937.8 | −4.09 | −16.22 | Normalization $CO_2$-scale |
| B2 | 441.1 | −4.09 | −16.22 | Normalization & calibration |
| C | 447.5 | −16.63 | −19.98 | Calibration $\delta$-scale |

TABLE 1    Calibration standards prepared for this study. The $\delta$-scales are given in VPDB and VPDB-$CO_2$ for $\delta^{13}C$ and $\delta^{18}O$, respectively

and a third one to define the calibration function that links the normalized isotope ratio values to the $\delta$-scale. A summary of the gases used in this study is given in Table 1. Their exact $\delta$-values were determined by high precision IRMS analysis and linked to the VPDB-$CO_2$ scale [32]. The $CO_2$ concentration of each tank was linked to the World Meteorological Organization (WMO) scale by infrared gas analysis (LI-7000, LI-COR). These calibrated concentration values were then used to check the linearity of the laser spectrometer over this range of $CO_2$ concentrations and to normalize the spectroscopically determined mixing ratios to the WMO scale.

Finally, it should be noted that fractionation processes during the dilution step can be excluded for two main reasons. First, if this would be a significant process, then the dilution of gases with high (but different) $CO_2$ concentrations and different isotope ratios would not yield a linear correlation (Fig. 4b) and second, the application of this calibration scheme would not give the correct values (compared to IRMS) when used on field samples with strong variations in total $CO_2$ (see Sect. 3).

## 2.4    Field measurements

*2.4.1 Study site and sampling system.*  The laser spectrometer participated in a field campaign (August 15 to 23, 2007) to demonstrate its potential application in carbon-cycle research by performing in situ, fast and continuous concentration measurements of the three main $CO_2$ isotopologues. The field experiments were conducted at the Chamau research station of the ETH Zurich located in Central Switzerland at 400 m a.s.l. ($47°12'34''N/8°24'36''E$). The observation area is situated at an intensively managed grassland on which a mixed rye grass-clover vegetation was raised for forage.

The instrument analyzed air samples collected from four different heights (0.05, 0.1, 0.4 and 2.1 m) above the ground to measure flux gradients. The sampling and calibration setup had a similar configuration as the one presented by Tuzson et al. [28]. It was slightly modified to adopt to the new optical system and to minimize the pressure transients during valve switching. Briefly, PTFE tubing (6 mm i.d.) conducted the air stream to the instrument which was located in a thermostatically controlled container at the edge of the field, a distance of approximately 60 m. The air samples were filtered first at the inlet by a Teflon membrane filter and secondly before entering the absorption cell using a 7 μm sintered metal filter. A heated and PTFE coated diaphragm vacuum pump (N036ST.26E, KNF) pulled the air through the tubing and maintained a constant flow of $\sim 6$ l/min. Since drying is essential to eliminate volumetric effects on mixing ratio determinations, as well as collisional broadening effects [14], the air from the pump outlet was directed through a Nafion drier (PD-100T, Perma Pure). A poppet check valve (SS-4CPA2-3, Swagelok), adjusted to 110 kPa, was added between the pump outlet and the Nafion based drier to avoid pressure build-up during sample–calibration switching. The air was then passed across the temperature controlled "cold plate" and continuously drawn through the multi-pass cell (sample side) at a pressure of 8 kPa. A flow rate of 400 ml/min was maintained by a scroll pump (TriScroll 300, Varian). The flow rates and pressures in both cells were controlled by a combination of thermal mass flow controllers (Red-y smart series, Vögtlin Instruments AG) and metering bellows-sealed valves (SS-4BMG, Swagelok) at the cell inlet and at downstream side, respectively.

The instrument's sampling system periodically switched between calibration gases and air sample. The measurement cycle was as follows: (1) standard tank A; (2) standard tank B1; (3) standard tank B2; (4) standard tank C; (5) air sample measurement above the soil surface at various heights. Within each 30 min cycle the calibration gases were sampled for 150 s each and the atmospheric inlet was sampled for 20 min. During the air-sampling interval an inlet manifold sequentially cycled between the four heights spending 150 s at each intake. Hence, the spectrometer analyzed each level twice within the sampling time. This cycling was applied to the sample cell only, while through the reference cell a continuous flow (180 ml/min) of reference gas (tank A) was maintained during the entire campaign.

*2.4.2 Mass spectrometry of the flask samples.* Additional to the QCLAS measurements, an automatic sampler for air (ASA) acquired, in two hours cycle, air samples over a 2 min interval. The $CO_2$ mixing ratios were measured by an IRGA (LI-840, LI-COR), while the $\delta^{13}C$ and $\delta^{18}O$ values were determined at the IsoLab (ETH Zurich) by GasBench II – IRMS (Delta$^{plus}$XP, Finnigan MAT). The ASA sample manifolds [33] were modified to our field and laboratory requirements to store desiccant (magnesium perchlorate) dried air samples in glass flasks (300 ml) or metal loops (10 ml). In the laboratory, a feed capillary delivered pure He to the ASA allowing a pressure build-up in the glass flasks which flushed the sample gas at a rate of about 5 ml/min over a Nafion dryer to the cryotrap operating at liquid nitrogen temperature. Here the condensable gases (mainly $CO_2$ and $N_2O$) were frozen

out. After diverting the non-condensable gases to vent, the cryotrap was allowed to warm-up and its content was injected into a GC column (Poraplot, Varian) held at 24 °C to allow separation of the $CO_2$ from $N_2O$. The carbon and oxygen isotopic composition of the $CO_2$ were expressed as the relative difference of its isotopic abundance ratio relative to that of an international standard. Post-run off-line calculation and drift correction for assigning the final $\delta^{13}C$ and $\delta^{18}O$ values on the V-PDB and V-PDB-$CO_2$ scale were done following the "IT principle" as described by Werner and Brand [34]. The accurate assigning of the $\delta^{13}C$ and $\delta^{18}O$-values of the laboratory standards to the V-PDB and the V-PDB-$CO_2$ scale was performed at the Max-Planck-Institut für Biogeochemie (Jena, Germany) by measuring them versus the "Jena-Reference AirSet" (J-RAS) as standard reference material [35].

## 3 Results and discussion

Time series of the $CO_2$ mixing ratio and the derived $\delta^{13}C$ as well as $\delta^{18}O$-values from the measurement height $z_2$ (0.1 m) are presented in Fig. 5. Each data point is an integrated value over 55 s. There were large changes in $CO_2$ concentration and $^{13}C$ (and $\delta^{18}O$)-values observed during diurnal time courses. Similar data sets were obtained for the other three intake heights as well. Their consistency can be easily assessed from Fig. 6, which reveals a strong vertical stratification of $CO_2$ concentration and isotopic composition, with higher concentrations and lower $\delta$-values, for both $^{13}C$ and $^{18}O$, observed closer to the soil surface. The diurnal changes are the results of isotope discrimination by the vegetation and turbulent mixing of canopy air and the boundary layer [36]. During daytime, photosynthetic $CO_2$ uptake exceeded respiration and $CO_2$ concentrations were reduced to about 40 ppm below ambient, and the atmospheric $CO_2$ became slightly enriched in $^{13}C$ ($\approx -6\text{‰}$). In contrast, at night, when the respiration processes dominated, atmospheric $CO_2$ concentration was increased (up to 2000 ppm) and its $^{13}C$ content was depleted ($\approx -26\text{‰}$). This depletion occurs because the original carbon fixed by plants is depleted in $^{13}C$ relative to atmospheric $CO_2$. The ability to simultaneously measure these changes in $CO_2$ concentration and its isotope ratios allows the separation of photosynthesis and respiration components of the net $CO_2$ exchange on local and regional scales [37]. Assuming that the measured $CO_2$ above the ecosystem is primarily a result of mixing between two sources, the atmosphere above the grassland and the $CO_2$ respired by plants and soils, it is possible to use a mass balance approach to calculate the isotope ratio of $CO_2$ respired by the ecosystem [6]. In agreement with the simple mixing model developed by Keeling, a plot of the measured $\delta^{13}C$ as a function of $1/[CO_2]$ gives a straight line relationship with the intercept $\delta^{13}C_r$, which represents the integrated measure of the isotopic composition of the $CO_2$ respired by the ecosystem. Figure 7 shows such a Keeling plot for data collected during 24 h at measurement height $z_2$. The $\delta^{13}C_r$ estimate is $-26.9 \pm 0.1\text{‰}$. For the regression, daytime and nighttime data were combined, which is reasonable to a first approximation for regional studies assuming that photosynthetic and respiratory processes are at equilibrium [38].

The same mixing model can also be used for oxygen isotope ratios of grassland air [37, 39, 40]. In this case the inter-
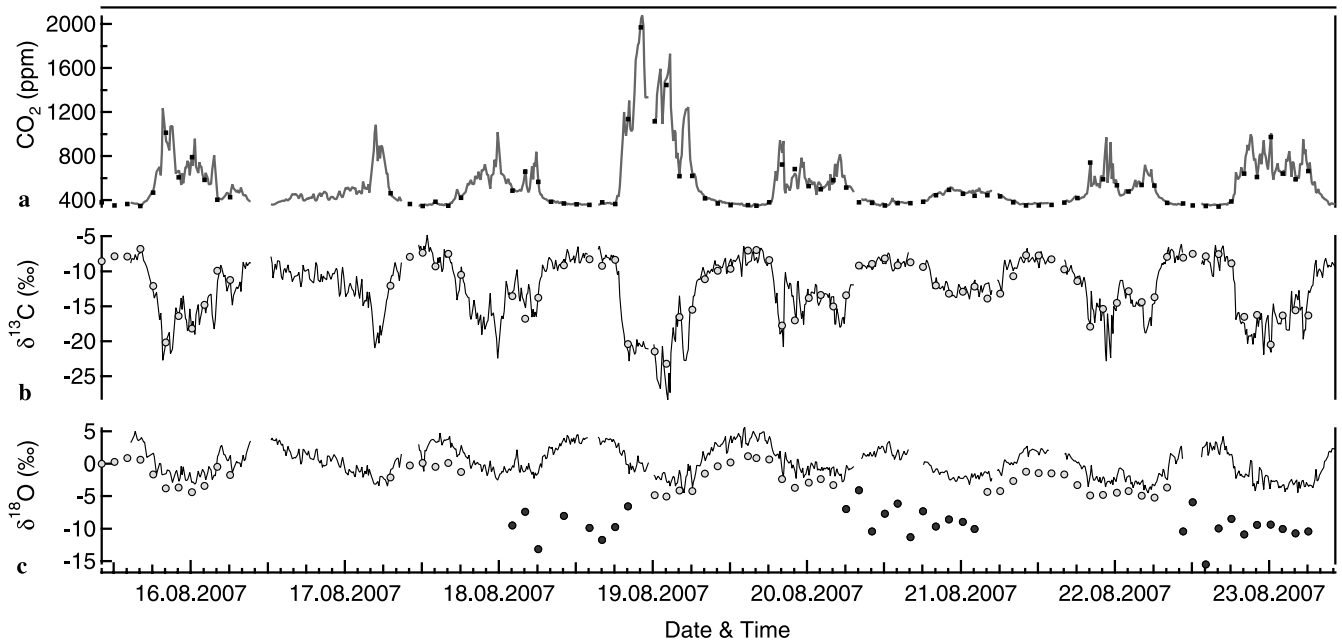
**FIGURE 5**   (**a**) Time series of the carbon dioxide mixing ratio measured by the QCLAS (*line*) and with an IRGA (*dots*). The corresponding $\delta^{13}$C and $\delta^{18}$O-values measured by the laser spectrometer are shown in (**b**) and (**c**). For comparison IRMS $\delta$-values are also given. The *closed symbols* for the $\delta^{18}$O-values indicate sampling issues with the metal flasks (details in text)
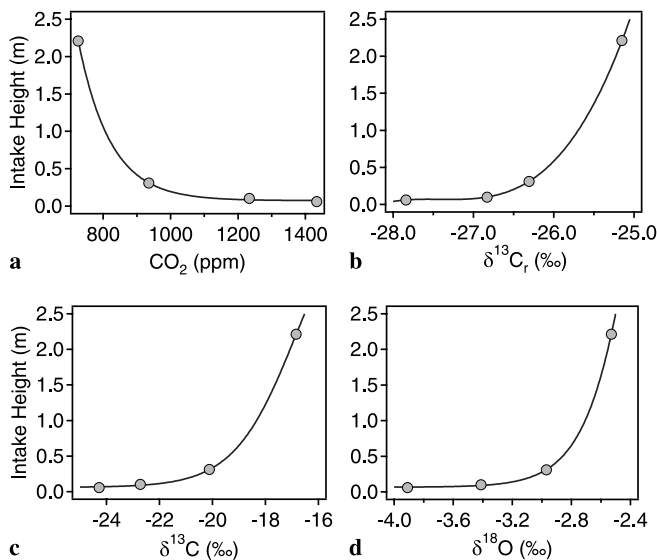


**FIGURE 6**   Vertical gradients in concentration (**a**) and isotopic composition (**c** and **d**) of $CO_2$ in the atmosphere above the grass land. (**b**) The vertical stratification was also mirrored in the ecosystem respiration signatures ($\delta^{13}C_r$) defined as the intercept of a Keeling plot

cept ($\delta^{18}O_r$) describes the oxygen isotope ratio of ecosystem respiratory $CO_2$, integrating leaf and soil respiration. It should be recognized, however, that the Keeling mixing model is less reliable at the ecosystem scale when applied to $^{18}$O because of the greater spatial heterogeneity in the oxygen isotope ratio of the source water in leaves and soil at relatively small spatial scales and dynamic variation among these components at short time scales. Despite of these limitations, the QCLAS delivered useful data about this $CO_2$ isotopologue. As illustrated in Fig. 5, the $\delta^{18}$O-values also show a systematic diurnal variation over the entire sampling period, a feature which is

supported by previous field studies [37, 39–41]. The slight increase during the course of the day is probably due to isotope exchange with enriched leaf water. In contrast, lower $\delta^{18}$O-values near to the soil surface might indicate isotope exchange of soil respired $CO_2$ with the more depleted soil water. A significant linear relationship between the $^{13}$C and $\delta^{18}$O-values of canopy air ($R^2 = 0.82$) has been found, which indicates a tight coupling between water vapor and carbon dioxide fluxes. More detailed interpretation of these data are beyond the scope of the present investigation and will be the subject of a separate paper. However, we stress on the fact that beyond the diurnal changes, there was considerable temporal variation in the isotopic composition of atmospheric $CO_2$ even during the course of a single night. Capturing this variation with flask collections and mass spectrometry would be impractical. Furthermore, the high temporal resolution of the QCLAS led to significantly more data points compared to IRMS, and so to much more constrained values for the ecosystem respiration. Representing the Keeling plot intercept as function of sampling height (see Fig. 6b) has only been made possible due to the fast and high precision isotope measurements achieved with the laser spectrometer. Moreover, considering the $\delta^{18}$O-values determined by IRMS from the flask air samples (see Fig. 5), it is obvious that they exhibit pronounced fluctuations, which do not correlate with any environmental variable, such as solar radiation, air temperature, relative humidity, etc., monitored on the field. It is known [42] that flask sampling systems are susceptible to problems related to storage of the air samples in volumes that have not thoroughly been preconditioned. The $\delta^{18}$O-values may suffer from isotope exchange effects between water and carbon dioxide. This idea is also supported by the clear negative trend of the $\delta$-values. Air samples collected in glass flasks show only a small negative bias in the measured $\delta^{18}$O-values, which is, however, much more accentuated for air samples stored in the smaller
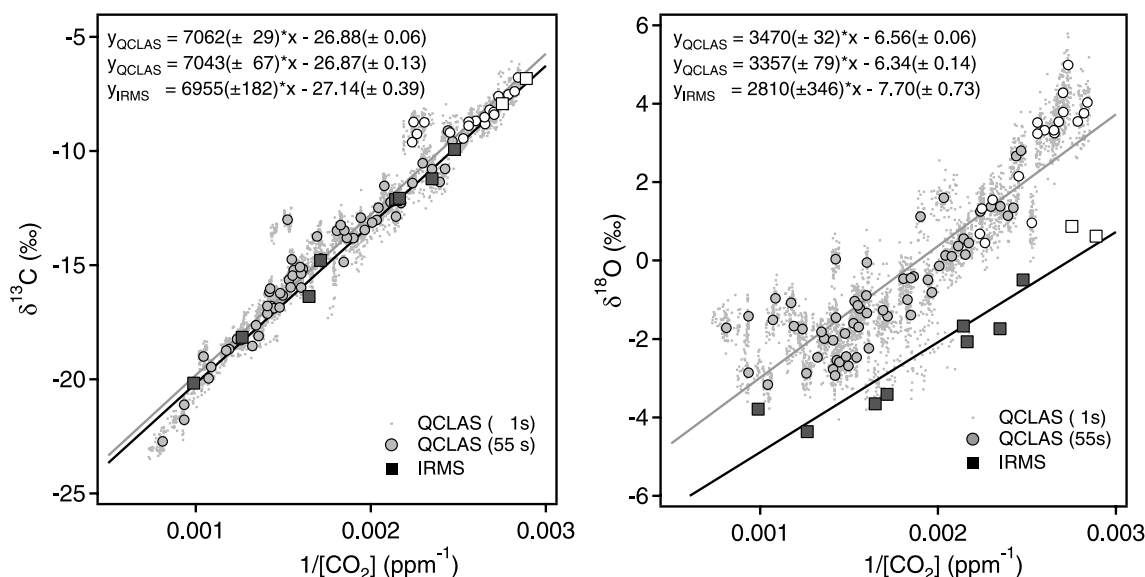
FIGURE 7 Keeling plots for data collected during 24 h at measurement height $z = 0.1$ m. Isotope ratios are plotted vs. the inverse of $CO_2$ concentration. The intercept and the slope of the linear regression is given together with their standard deviation. Besides the QCLAS data points (*circles*), the field-collected flask samples are also plotted (*rectangles*). The day- and nighttime measurements are indicated by *open* and *closed symbols*, respectively. The one second QCLAS data are also presented in the background (*dots*)
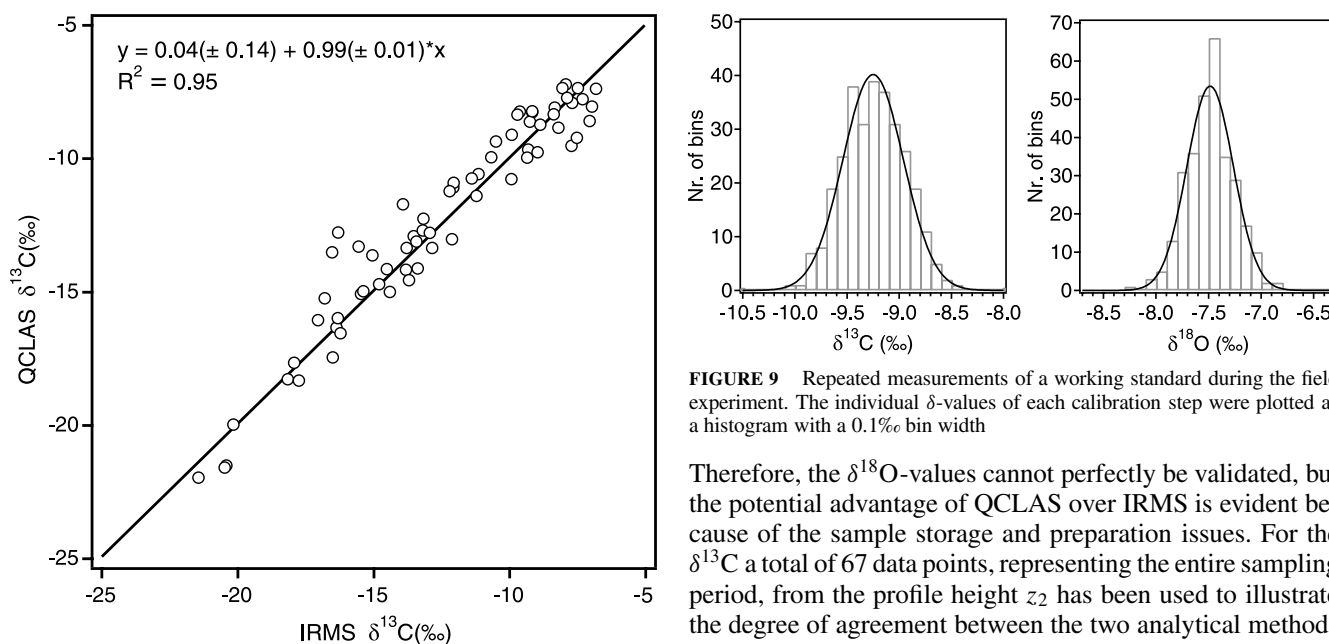


FIGURE 8 Comparison of $^{13}C$-values measured with QCLAS and IRMS. Flask samples for the IRMS were collected every 2 h during the experimental period (August 15–23, 2007). The linear regression indicates an excellent agreement between the two techniques



FIGURE 9 Repeated measurements of a working standard during the field experiment. The individual $\delta$-values of each calibration step were plotted as a histogram with a 0.1‰ bin width

metal tube volumes. For future investigations, a proper selection of flask material and their careful pretreatment is clearly needed before sampling.

Since the flask system shared the same inlet as the QCLAS sample system, a direct comparison of the $\delta^{13}C$-values measured by IRMS and the QCLAS could be performed. This is, however, not the case for the $\delta^{18}O$-values, because of the probability of oxygen isotope exchange between water and carbon dioxide mentioned above. Here, the storage and reaction time (several hours) of the sample gas in the flasks is not the same as the sampling/analyzing time (few seconds) of the QCLAS.

Therefore, the $\delta^{18}O$-values cannot perfectly be validated, but the potential advantage of QCLAS over IRMS is evident because of the sample storage and preparation issues. For the $\delta^{13}C$ a total of 67 data points, representing the entire sampling period, from the profile height $z_2$ has been used to illustrate the degree of agreement between the two analytical methods (Fig. 8). The intercept clearly indicates that there is no significant isotope fractionation effect for the $^{13}CO_2$ during the sampling procedure.

Beyond the field data presented above, the periodic measurement of the calibration gases during the whole campaign can be used for a straightforward estimate of the replicate precision and accuracy of the isotope ratio measurements under field conditions. As described in Sect. 2.3, the retrieved isotope ratios were calibrated by relying on three calibration gases (A, B2 and C, listed in Table 1), which have similar $CO_2$ concentrations but different isotopic compositions. These gases were used together to determine the linear calibration function that links the measured isotope ratios to the $\delta$-scale (similar to Fig. 4b). To asses the instrument's stability, a calibration function was determined using two reference gases only (B2 and C) while treating the third (A) as

an external standard. The histogram of all available $\delta$-values ($N = 301$) validated for gas A over the entire sampling period has a nearly normal distribution (Fig. 9). This is illustrated by the Gaussian distribution shown in the same figure, which was generated based on the mean value ($-9.25$ and $-7.48‰$ for $\delta^{13}C$ and $\delta^{18}O$, respectively) and the $1\sigma$ standard deviation ($0.29$ and $0.22$) of the repeated measurements. These results indicate that both precision and accuracy are about $0.2‰$ and can routinely be obtained if all calibration gases are used, as it was the case for the campaign. Since this describes the statistical uncertainty of single values, repeated measurements may lead to a much lower error of the mean. This is highly relevant for the measurements of ambient air at remote locations where changes are very slow, and averaging may permit to determine $\delta$-values with even better accuracy.

## 4    Conclusions

This paper demonstrates the real benefits of using infrared laser absorption spectroscopy for in situ, fast and high precision isotope measurements of $CO_2$ at ambient mixing ratios. The instrument, employing cryogenic-free components for both laser and detector, can be operated unattended in the field to provide continuous and simultaneous measurements of $^{12}CO_2$, $^{13}CO_2$ and $^{16}O^{12}C^{18}O$ concentrations. Combining a standard optical concept with the spectral ratio approach it was possible to measure two isotope ratios with a precision of $0.24$ and $0.29‰$, for an acquisition time of $1$ s. Signal averaging of $\sim 100$ s further improves the instrumental performance and leads to a precision well below $0.1‰$. Furthermore, the rapid sampling provides the opportunity to investigate the temporal dynamics of the discrimination mechanisms controlling ecosystem–atmosphere $CO_2$ exchange. Merging the isotope ratio analysis with dynamic flux measurements using the eddy-covariance technique is already in our research agenda. A robust calibration scheme assures an accuracy of better than $0.2‰$ to be routinely obtained for the isotope ratios in long-term field measurements. Replicate measurements of a reference gas reveals that a mean $\delta$-value with an error of about $0.02‰$ can be obtained. This clearly points towards the feasibility to apply the instrument for the investigation of interannual and seasonal variations of atmospheric $CO_2$.

## REFERENCES

1  S. Solomon, D. Qin, M. Manning, Z. Chen, M. Marquis, K.B. Averyt, M. Tignor, H.L. Miller (Eds.), *IPCC, 2007: Climate Change 2007: The Physical Science Basis* (Cambridge University Press, Cambridge, 2007)
2  P.P. Tans, I.Y. Fung, T. Takahashi, Science **247**, 1431 (1990)
3  M. Trolier, J.W.C. White, P.P. Tans, K.A. Masarie, P.A. Gemery, J. Geophys. Res. **101**, 25 897 (1996)
4  T.J. Conway, P.P. Tans, L.S. Waterman, K.W. Thoning, D.R. Kitzis, K.A. Masarie, N. Zhang, J. Geophys. Res. **99**, 22 831 (1994)
5  C.D. Keeling, J.F.S. Chin, T.P. Whorf, Nature **382**, 146 (1996)
6  C.D. Keeling, Geochim. Cosmochim. Acta **13**, 322 (1958)
7  G.D. Farquhar, J. Lloyd, J.A. Taylor, L.B. Flanagan, J.P. Syvertsen, K.T. Hubick, S.C. Wong, J.R. Ehleringer, Nature **363**, 439 (1993)
8  P. Ciais, P.P. Tans, M. Trolier, J.W.C. White, R.J. Francey, Science **269**, 1098 (1995)
9  D. Nelson, J.B. McManus, S.C. Herndon, M.S. Zahniser, B. Tuzson, L. Emmenegger, Appl. Phys. B **90**, 301 (2008)
10  P. Bergamaschi, M. Schupp, G.W. Harris, Appl. Opt. **33**, 7704 (1994)
11  G. Gagliardi, R. Restieri, G. Casa, L. Gianfrani, Opt. Lasers Eng. **37**, 131 (2002)
12  J. Zhang, T.J. Griffis, J.M. Baker, Plant Cell Environ. **29**, 483 (2006)
13  T.J. Griffis, J.M. Baker, S.D. Sargent, B.D. Tanner, J. Zhang, Agric. For. Meteorol. **124**, 15 (2004)
14  D.R. Bowling, S.D. Sargent, B.D. Tanner, J.R. Ehleringer, Agric. For. Meteorol. **118**, 1 (2003)
15  H. Waechter, M.W. Sigrist, Appl. Phys. B **87**, 539 (2007)
16  M. Erdelyi, D. Richter, F.K. Tittel, Appl. Phys. B **75**, 289 (2002)
17  P. Bergamaschi, M. Schupp, G.W. Harris, Appl. Opt. **33**, 7704 (1994)
18  J.B. McManus, M.S. Zahniser, D.D. Nelson, L.R. Williams, C.E. Kolb, Spectrochim. Acta A **58**, 2465 (2002)
19  K. Uehara, K. Yamamoto, T. Kikugawa, N. Yoshida, Spectrochim. Acta A **59**, 957 (2003)
20  C. Janssen, B. Tuzson, Appl. Phys. B **82**, 487 (2006)
21  E.R.T. Kerstel, R. van Trigt, N. Dam, J. Reuss, H.A.J. Meijer, Anal. Chem. **71**, 5297 (1999)
22  E.D. Murnick, J.O. Okil, Isotope Environ. Health Stud. **41**, 363 (2005)
23  J.B. McManus, D.D. Nelson, J.H. Shorter, R. Jimenez, S. Herndon, S.R. Saleska, M.S. Zahniser, J. Mod. Opt. **52**, 2309 (2005)
24  D. Weidmann, C.B. Roller, C. Oppenheimer, A. Fried, F.K. Tittel, Isotope Environ. Health Stud. **41**, 293 (2005)
25  A.A. Kosterev, R.F. Curl, F.K. Tittel, C. Gmachl, F. Capasso, D.L. Sivco, J.N. Baillargeon, A.L. Hutchinson, A.Y. Cho, Opt. Lett. **24**, 1762 (1999)
26  J.B. McManus, D.D. Nelson, S.C. Herndon, J.H. Shorter, M.S. Zahniser, S. Blaser, L. Hvozdara, A. Muller, M. Giovannini, J. Faist, Appl. Phys. B **85**, 235 (2006)
27  D.D. Nelson, J.H. Shorter, J.B. McManus, M.S. Zahniser, Appl. Phys. B **75**, 343 (2002)
28  B. Tuzson, M.J. Zeeman, M.S. Zahniser, L. Emmenegger, Infrared Phys. Technol. **51**, 198 (2008)
29  P. Werle, R. Mucke, F. Slemr, Appl. Phys. B **57**, 131 (1993)
30  L.S. Rothman, D. Jacquemart, A. Barbe, D.C. Benner, M. Birk, L.R. Brown, M.R. Carleer, C. Chackerian, K. Chance, L.H. Coudert, V. Dana, V.M. Devi, J.-M. Flaud, R.R. Gamache, A. Goldman, J.-M. Hartmann, K.W. Jucks, A.G. Maki, J.-Y. Mandin, S.T. Massie, J. Orphal, A. Perrin, C.P. Rinsland, M.A.H. Smith, J. Tennyson, R.N. Tolchenov, R.A. Toth, J. Vander Auwera, P. Varanasi, G. Wagner, J. Quantum Spectrosc. Radiat. Transf. **96**, 139 (2005)
31  J. Mohn, R.A. Werner, B. Buchmann, L. Emmenegger, J. Mol. Struct. **834–836**, 95 (2007)
32  R.A. Werner, W.A. Brand, Rapid Commun. Mass. Spectrom. **15**, 501 (2001)
33  D.E. Theis, M. Saurer, H. Blum, E. Frossard, R.T.W. Siegwolf, Rapid Commun. Mass. Spectrom. **18**, 2106 (2004)
34  R.A. Werner, M. Rothe, W.A. Brand, Rapid Commun. Mass. Spectrom. **15**, 2152 (2001)
35  P. Ghosh, M. Patecki, M. Rothe, W.A. Brand, Rapid Commun. Mass. Spectrom. **19**, 1097 (2005)
36  G.D. Farquhar, J.R. Ehleringer, K.T. Hubick, Ann. Rev. Plant. Physiol. Plant Mol. Biol. **40**, 503 (1989)
37  D. Yakir, X.F. Wang, Nature **380**, 515 (1996)
38  D.E. Pataki, J.R. Ehleringer, L.B. Flanagan, D. Yakir, D.R. Bowling, C.J. Still, N. Buchmann, J.O. Kaplan, J.A. Berry, Global Biogeochem. Cycl. **17**, 1022 (2003)
39  L.B. Flanagan, J.R. Brooks, G.T. Varney, J.R. Ehleringer, Global Biogeochem. Cycl. **11**, 83 (1997)
40  N. Buchmann, J.R. Ehleringer, Agric. For. Meteorol. **89**, 45 (1998)
41  L.B. Flanagan, G.T. Varney, Oecologia **101**, 37 (1995)
42  P.A. Gemery, M. Trolier, J.W.C. White, J. Geophys. Res. **101**, 14 415 (1996)